$CsPbBr_3$ perovskites: Theoretical and experimental investigation on water-assisted transition from nanowire formation to degradation

B. Akbali,[1] G. Topcu,[2] T. Guner,[2] M. Ozcan,[3] M. M. Demir,[2] and H. Sahin[3,4,*]

[1]*Department of Physics, Izmir Institute of Technology, 35430, Izmir, Turkey*

[2]*Department of Materials Science and Engineering, Izmir Institute of Technology, 35430, Izmir, Turkey*

[3]*Department of Photonics, Izmir Institute of Technology, 35430, Izmir, Turkey*

[4]*ICTP-ECAR Eurasian Center for Advanced Research, Izmir Institute of Technology, 35430, Izmir, Turkey*

(Received 15 January 2018; published 5 March 2018)

Recent advances in colloidal synthesis methods have led to an increased research focus on halide perovskites. Due to the highly ionic crystal structure of perovskite materials, a stability issue pops up, especially against polar solvents such as water. In this study, we investigate water-driven structural evolution of $CsPbBr_3$ by performing experiments and state-of-the-art first-principles calculations. It is seen that while an optical image shows the gradual degradation of the yellowish $CsPbBr_3$ structure under daylight, UV illumination reveals that the degradation of crystals takes place in two steps: transition from a blue-emitting to green-emitting structure and and then a transition from a green-emitting phase to complete degradation. We found that as-synthesized $CsPbBr_3$ nanowires (NWs) emit blue light under a 254 nm UV source. Before the degradation, first, $CsPbBr_3$ NWs undergo a water-driven structural transition to form large bundles. It is also seen that formation of such bundles provides longer-term environmental stability. In addition theoretical calculations revealed the strength of the interaction of water molecules with ligands and surfaces of $CsPbBr_3$ and provide an atomistic-level explanation to a transition from ligand-covered NWs to bundle formation. Further interaction of green-light–emitting bundles with water causes complete degradation of $CsPbBr_3$ and the photoluminescence signal is entirely quenched. Moreover, Raman and x-ray-diffraction measurements revealed that completely degraded regions are decomposed to $PbBr_2$ and CsBr precursors. We believe that the findings of this study may provide further insight into the degradation mechanism of $CsPbBr_3$ perovskite by water.

DOI: 10.1103/PhysRevMaterials.2.034601

I. INTRODUCTION

Halide perovskites, having the structure ABX_3 [where A is organic: $CH_3NH_3^+$ (MA), $HC(NH_2)_2^+$ (FA), or inorganic: Cs^+ cation, B a metal cation: Pb^{2+}, Sb^{2+}, Sn^{2+}, and X a halide anion: Cl^-, I^-, Br^-], have been known since the 1950s [1]. With the discovery of $MAPbI_3$ as a photosensitizer in dye-sensitized solar cells in 2009 [2], these materials have started to receive more attention [3]. Since then, in a short time, perovskite solar cells have become able to improve the conversion efficiency from 3.81% to almost 20% [2,4–6]. Apart from the success of these materials in photovoltaic applications [7], it has been demonstrated recently that these materials can be applied also to light-emitting diodes [8–10], lasers [11,12], photodetectors [13], etc. due to their unique optical properties: high quantum yield (90%), wavelength tunability, and color purity [14–19].

Even though all-inorganic perovskites are better in terms of intrinsic stability than the organometallic halide ones, stability is still a challenge, especially against moisture and polar solvents such as water, ethanol, acetone, etc. [14,19–21]. Such high chemical instability mainly stems from the high ionic character of the compounds. However, practical applications require a deeper understanding of degradation mechanisms for synthesis of highly stable halide perovskites under ambient conditions. To date, various approaches have been developed such as mixing with mesoporous silica [22], a core-shell structure [23–25], different surface treatments [other than usual ones; oleic acid (OA), and oleylamine (OAm)] [26,27], or encapsulation with polymers [28–30] to obtain perovskite nanocrystals with high stability.

Recently, among halide perovskites, all-inorganic $CsPbX_3$ nanocrystals have started to draw much attention because of their high photoluminescence quantum yields and controllable morphologies [31–34]. Chen *et al.* reported an efficient synthesis technique to prepare $CsPbX_3$ nanocrystals with tunable composition, luminescence characteristics, and morphologies [35].

Degradation mechanisms at the atomic level and possible stabilization techniques are still open questions in the growing field of perovskite nanocrystals. A very recent study by Yuan *et al.* reported that both light and humidity may degrade $CsPbI_3$ quantum dots [36]. A recent perspective study on lead halide perovskite solar cells (PSCs) enlightens the defect tolerance and stability of the material [20]. Lejitas and co-workers reviewed strategies to overcome the issues of structural, thermal, and atmospheric degradation of $CsPbX_3$ nanocrystals [37]. In addition to experimental studies, tremendous efforts have been also performed on PSCs by carrying out density functional theory calculations [38–42]. Kang *et al.* theoretically predicted that for its electronic properties $CsPbBr_3$ is a defect-tolerant

*hasansahin@iyte.edu.tr

semiconductor [43]. In addition, theoretical studies on defects in perovskites have been widely performed [44–47]. Although the organic-inorganic hybrid lead halide perovskites have been studied theoretically and experimentally, the pure inorganic alternative, the $CsPbBr_3$ phase, has been recently found to possess most of the good properties of the hybrid lead halide counterpart [18,48].

The paper is organized as follows: Detailed information about computational and experimental methodologies is given in Sec. II. Characteristic properties of as-synthesized $CsPbBr_3$ are investigated in Sec. III. Water-assisted transition from blue- to green-emitting structure is explained in Sec. IV, and complete degradation of the perovskite material is discussed in Sec. V. Finally, we conclude in Sec. VI.

II. METHODOLOGY

A. Experimental methodology

Cesium carbonate (Cs_2CO_3, 99.9%, Sigma-Aldrich), lead (II) bromide ($PbBr_2$, $\geqslant$98%, Sigma-Aldrich), oleic acid (OA, 90%, Alfa Aesar), oleylamine (OLA, 90%, Sigma-Aldrich), 1-octadecene (ODE, 90%, Sigma-Aldrich), dimethylformamide (DMF, $\geqslant$99.9%, Tekkim), hexane ($\geqslant$98%, Sigma-Aldrich), and acetone (Merck, $\geqslant$99.5%) were purchased and used as received without any further purification. Oxidized silica substrate was purchased from University Wafers.

Synthesis of Cs-oleate: Cs-oleate solution was synthesized with slight modifications by following Amgar *et al.* [49]; Cs_2CO_3 (0.2 g), OA (625 μl) and ODE (7.5 ml) were loaded into three necked flasks and dried under vacuum (150 mbar) at 120 °C for 1 h. Subsequently, the mixture was heated to 150 °C under N_2, and the reaction was maintained until all Cs_2CO_3 was consumed by OA. Afterwards, the yellowish Cs-oleate solution was gradually cooled down (it has to be preheated to 100 °C before using).

Synthesis of $CsPbBr_3$: $CsPbBr_3$ crystals were prepared in four steps with slight modifications based on the procedure in Ref. [49]. An aliquot of 0.125 ml OA, 0.125 ml OLA, and 1.25 ml ODE were loaded into a glass vial. Subsequently, 0.1 ml of preheated Cs-oleate solution was added to the mixture, and addition of 0.2 ml of $PbBr_2$ precursor solution (0.4 M, heated for 1 h at 80 °C until full dissolution) followed. After 10 s, 5 ml of acetone was rapidly added to trigger the crystallization of the $CsPbBr_3$. Stirring was maintained for 30 min, and green precipitates were collected by using centrifuge (6000 rpm, 10 m). Precipitates were redispersed in hexane.

Preparation of water contact $CsPbBr_3$ surface: First, 150 μl $CsPbBr_3$−hexane dispersion was cast on an oxidized silica substrate (approximately 1 cm^2). $CsPbBr_3$ structures were formed immediately after the quick evaporation of hexane. Second, an aliquot of distilled water was put over the $CsPbBr_3$-coated silica substrate, and we waited till the water completely evaporated. Characterizations were carried out in ambient conditions. For further aging of the crystals, water-driven transitions were conducted by adding the desired amount of water. Water contact time was recorded as the total time of exposure.

The diffraction profile of the $CsPbBr_3$ structures was recorded with an x-ray diffractometer (X'Pert Pro, Philips, Eindhoven, the Netherlands). Scanning electron microscopy (SEM; Quanta 250, FEI, Hillsboro, OR, USA) was used to determine $CsPbBr_3$ morphology in back-scattering electron detectors. Images of the degraded crystals were captured via an optical microscope (BX 53, Olympus, Tokyo, Japan). Emission spectra were determined with a USB2000+ spectrometer (Ocean Optics Inc., Dunedin, FL, USA) via a premium fiber cable. Raman spectroscopy (Horiba Xplora Plus) was used to determine fingerprint Raman-active vibrations of $CsPbBr_3$ structures. Absorption was collected using an Olympus (CX-31) optical microscope integrated with a USB2000 + spectrometer.

B. Computational methodology

To investigate interaction between Cs- and Pb-rich surfaces of orthorhombic $CsPbBr_3$ with water, OA, and OAm molecules, we performed density functional theory-based calculations using the projector augmented wave [50,51] potentials as implemented in the Vienna *ab initio* Simulation Package [52,53]. The local density approximation (LDA) [54] was used with the inclusion of spin-orbit coupling to describe the exchange and correlation potential as parametrized by the Ceperley and Alder functional to describe the exchange and correlation potential [55]. The Bader technique was used to analyze the partial charge transfer on the atoms [56].

A plane-wave basis set with kinetic energy cutoff of 500 eV was used for all the calculations. The total energy difference between the sequential steps in the iterations was taken to be 10^{-5} eV for the convergence criterion. The total force in the unit cell was reduced to a value of less than 10^{-4} eV/Å. Γ-centered k-point meshes of $3 \times 3 \times 3$ were used. A vacuum space of 10 Å was incorporated to avoid interaction with adjacent surfaces. Gaussian smearing of 0.1 eV was used for the electronic density of states calculations. Spin-polarized calculations were performed in all cases.

III. RESULTS

Structural and electronic evolution of the water-interacting $CsPbBr_3$ crystals were captured under both daylight and UV light (254 nm) at different times and the results shown in Fig. 1. First, silica substrates were identified as neatly showing as black under both daylight and UV. After dropping the $CsPbBr_3$-hexane dispersion over the substrate, the sample was observed to become green and yellowish-like under daylight and explicitly blue under UV. After interacting with water molecules about 24 h, as shown in Fig. 1(b), $CsPbBr_3$ turn explicitly greenish with some white crystals moving around expanding the sample volume, which exhibits a green emission covering a large area while leaving a small region as emitting blue under UV light. Further interaction with water leads to formation of white and relatively large crystals that do not exhibit luminescence under UV illumination due to possible degradation [Figs. 1(c) and 1(d)]. Monitoring the degradation under UV light reveals that degradation occurs in two different steps: formation of a green-emitting phase and complete degradation. Therefore, the following sections are devoted to experimental and atomic-level understanding of degradation of $CsPbBr_3$ crystals by water.

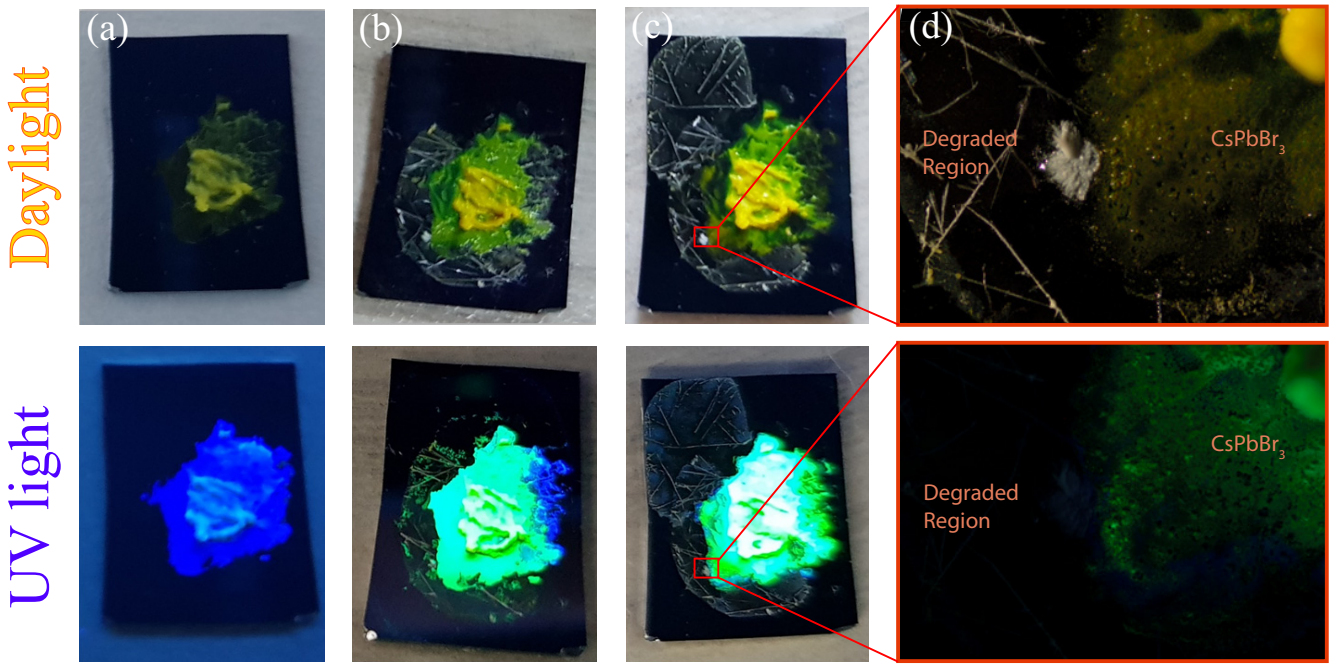

FIG. 1. Appearance of $CsPbBr_3$ under daylight and UV illumination; (a) initially after casting and (b) after 24 and (c) 144 h treated with water, respectively. Focused region in (c) presents the optical microscope image of the related sample under daylight and UV excitation.

A. Characteristic properties of blue light–emitting $CsPbBr_3$

$CsPbX_3$ nanocrystals exhibit three different structural phases: cubic (Pm-3m), orthorhombic (Pnma), and tetragonal (P4/mbm) [57–59]. At room temperature, $CsPbBr_3$ has been shown to possess a thermodynamically preferred orthorhombic structure [60]. In our calculations, structural properties of orthorhombic $CsPbBr_3$ are investigated, as seen in Fig. 2(a). Structural analysis reveals that optimized lattice parameters of bulk $CsPbBr_3$ are $a = 8.34$ Å, $b = 7.89$ Å, and $c = 11.29$ Å. Each Br atom bonds with two Pb atoms with a bond length of 2.92 Å. The Br-Pb-Br bond angle varies between 85° and 90°. Bader charge analysis shows that each Br atom receives $0.6e$/atom from Cs ($0.8e$/atom) and Pb ($1e$/atom) atoms. In addition, it is seen that the bond between Pb and Br atoms has a strong ionic character. On the other hand, Cs atoms slightly bind to the other atoms in the system even though the system receives a charge from Cs atoms.

The SEM image presented in Fig. 2(b) shows the morphological characteristics of $CsPbBr_3$ crystals. It is observed that the crystals, even though they have negligible aggregation, possess a one-dimensional shape. Selecting the individual ones from the image reveals that these nanowires (NWs) have a nanoscale diameter (∼50 nm) and submicron lengths (∼0.5–1.5 μm).

Raman measurement performed at room temperature with 785 nm laser excitation shows that $CsPbBr_3$ has five Raman-active modes as presented in Fig. 2(c). The vibration of the metal-halide sublattice, a prominent peak of $CsPbBr_3$, is measured at 72 cm^{-1}. According to a previous Raman study of the $CsPbCl_3$ crystal with *Pnma* phase [61], the peak at 72 cm^{-1} is assigned to the vibrational mode of $[PbBr_6]^{4-}$ octahedron and motion of Cs^+ cations. Moreover, it is seen that additional peaks appear at 46, 68, 83, and 102 cm^{-1}.

For further information on the crystal structure, the x-ray-diffraction (XRD) pattern of $CsPbBr_3$ NWs is presented in the inset of Fig. 2(c). The diffraction pattern is in good

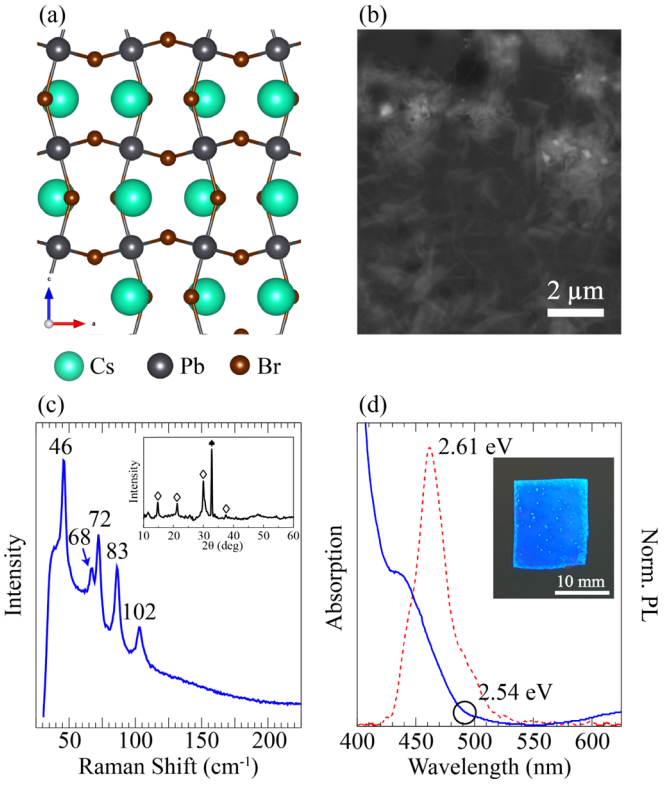

FIG. 2. (a) Crystal structure, (b) SEM image, (c) Raman measurement (inset: XRD pattern), and (d) photoluminescence and absorption spectra (inset: photograph under 254 nm UV light) of $CsPbBr_3$ NWs.

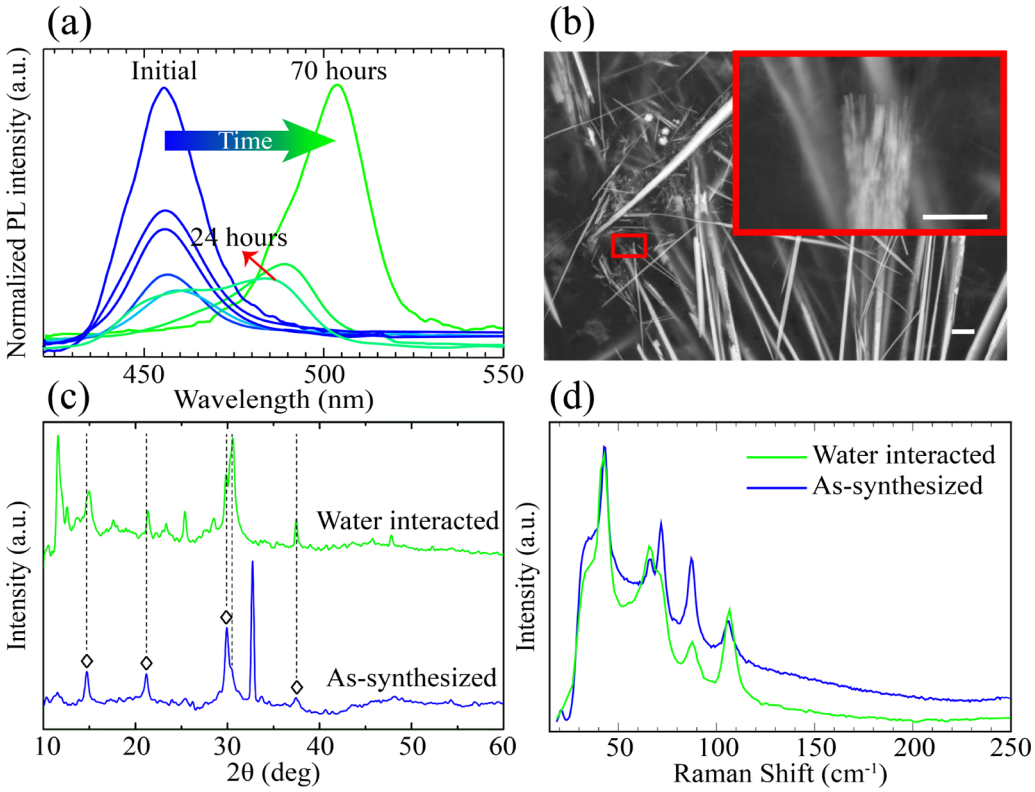

FIG. 3. (a) Time-dependent photoluminescence of as-synthesized NWs interacting with water, (b) SEM image of the resulting NW structure after 24 h of interaction, and (c)–(d) XRD measurement and Raman spectra of both as-synthesized and water-interacted samples. Scale bars are 2 μm.

agreement with the standard orthorhombic phase as the crystal structure of $CsPbBr_3$, where 2θ at 15°, 22°, 30°, and 31° reflections, marked with tilde symbol, correspond to the (110), (020), (004), and (220) planes, respectively [59]. The peak at 33° is due to a silicon wafer. Among the reflections, asymmetry between the (004) and (220) planes indicates a good morphological support in the sense of producing NW geometry.

The optical band gap of $CsPbBr_3$ NWs was determined via absorption spectrum, as shown in Fig. 2(d). Based on the data presented there, NWs show a broad range of absorption starting from a wavelength of ~488 nm, which follows an increasing trend with the decreasing wavelength. The absorption rate grows almost exponentially below ~425 nm. To estimate the band gap, the wavelength of where the absorption begins is considered, which gives a rough value of about 2.54 eV. The band gap, which corresponds to a wavelength of 488 nm, is verified by the photoluminescence (PL) spectrum, which is given with a dashed line in Fig. 2(d), of the NWs. In that spectrum, it is observed that NWs have narrow (FWHM = 38 nm) blue emission with maximum PL intensity at 475 nm under 254 nm UV light. The wavelength, which corresponds to 2.61 eV, is very close to the estimated band gap value above. For visualization, a photograph of the cast $CsPbBr_3$ NWs over a silica substrate under UV illumination, which is an explicit blue, is presented as the inset of Fig. 2(d).

B. Water-assisted transition from blue to green light–emitting structure

While $CsPbBr_3$ preserves its yellowish color during the water treatment, the water-driven transition into the green-emitting phase can be observed under UV. As shown in Fig. 3(a), the transition from blue to green emission due to water was recorded with different times. After 24 h, emission consists of two distinct signals: one signal around 450 nm represents the individual NWs [verifies the blue region in Fig. 1(b)], and a signal around 500 nm (greenish) indicates a significant redshift. From 24 to 70 h, the blue signal reduces and finally disappears while the greenish signal increases and dominates as a single signal at last.

The SEM image shown in Fig. 3(b) reveals formation of larger crystals that were grown particularly in a longitudinal direction compared to individual NWs, reaching >5 μm. The inset demonstrates an image that was taken with higher magnification over the edge of one of these crystals. It was observed that the tip of a large and rodlike crystal consists of many NWs, and the inset of Fig. 3(b) verifies the bundle formation through individual NWs. Therefore, the water-driven redshift in emission clearly stems from the quantum size effect, which is led by the structural transition from NW to bundle.

The crystal structure of green-emitting $CsPbBr_3$ was determined by XRD measurements, as shown in Fig. 3(c). The 2θ reflections at 15°, 22°, 30°, and 31° confirm that blue- and green-emitting phases correspond to the same crystal

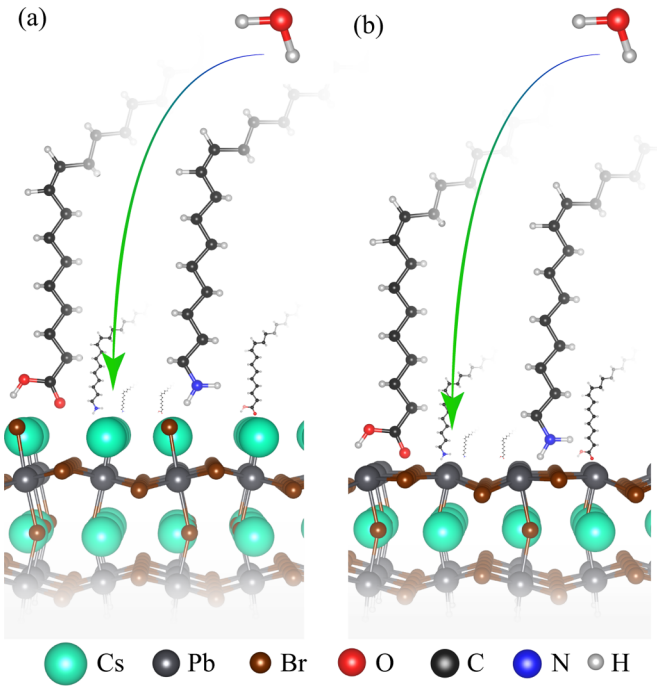

FIG. 4. Side views of (a) Cs-terminated and (b) Pb-terminated $CsPbBr_3$ surface.

structure. However, emergence of additional 2θ reflections at 12° and 25° are an indication of locally formed Cs_4PbBr_6 [62]. Raman spectra of green-emitting $CsPbBr_3$ bundles show that the prominent peak at 72 cm^{-1} and the other four modes still exist, as presented in Fig. 3(d). Raman activity of the water-interacted region is the same with as-synthesized $CsPbBr_3$ crystals. Therefore, vibrational characteristics of $CsPbBr_3$ NWs remains unchanged through the bundle formation.

Here, for deeper understanding of the water-driven NW-to-bundle transformation, we employ state-of-the-art first principles calculations. In order to examine all possible surfaces, we truncated bulk orthorhombic $CsPbBr_3$ at Cs and Pb surfaces as shown in Figs. 4(a) and 4(b). Both surfaces are saturated with H atoms to evade possible magnetization in the system.

For the surface cut from Cs atoms, the bond angle between Pb and Br atoms is calculated to be the same as the bulk form. Due to the surface relaxation, the Pb-Br bond length varies between 2.86 and 2.94 Å. In addition, Bader charge analysis reveals that the Pb atom donates (1.1e) to Br atoms (0.5–0.6e). Pb atoms donate 0.1e more compared with bulk $CsPbBr_3$. For the Pb truncated surface, it is clearly seen that there is a surface reconstruction where Pb-Br atoms make a line (∼180°), as shown in Fig. 4(b). Bond length Pb-Br atoms vary between 2.82 and 2.95 Å, which is wider range than the Cs surface. Bader charge analysis of Pb-terminated surface reveals that while Pb atoms donate 1.1e, Br atoms receive 0.5–0.6e.

Total energy optimization calculations for relaxation of H_2O molecules on two different surfaces show that water molecules prefer to bind on the bridge site on the Pb-Br bond. In addition, H_2O molecules bind to both surfaces via lone pairs of O atoms. For the Cs-terminated surface, the bond length between O and Cs atoms is calculated to be 2.91 Å. Charge analysis shows that the H_2O molecule receives 0.2e from the Cs atom. Binding energy (E_b) of the molecule is calculated to be 649 meV. The H_2O molecule is bound to the Pb atom with a bond length of 2.53 Å. The molecule prefers to bind the surface through the O atom without charge transfer between the molecule and the surface. On this surface, the E_b of the molecule is calculated to be 808 meV. Apparently, H_2O molecules strongly interact with the different surfaces of $CsPbBr_3$.

We also calculated the interactions between surface ligands, OA and OAm, with the NW surfaces. Optimized structures of the ligands are shown in Fig. 4. On the Cs-terminated surface, E_b of OA is calculated to be 698 meV. On the other hand, E_b of a water molecule on the same surface is calculated as 649 meV, and it is comparable with the OA binding energy. In addition E_b of OAm on the same surface is found to be 463 meV. For a Pb-terminated surface, the binding energy of OAm is calculated to be 874 meV. It is comparable with a H_2O molecule's binding energy (808 meV) on the same surface. Furthermore, the binding energy of OA molecule is found to be 221 meV.

To provide a complete discussion, interaction of water with ligands is also taken into account. It is found that E_b of H_2O with OA and OAm is calculated to be 898 and 550 meV, respectively. It can be concluded that oleic acid is more likely to bind with a water molecule than any other surface of $CsPbBr_3$. So H_2O molecules mediate the detachment of OA molecules from the surface of the NWs. Hence, a minor phase transformation from $CsPbBr_3$ to Cs_4PbBr_6 may arise from lack of OA that leads to excessive OAm on the surface of the NWs [63].

As a result, the binding energies of water and ligands on the surface of $CsPbBr_3$, which are comparable to each other, reveal that water is responsible for the removal of ligands over the $CsPbBr_3$ surface. It appears that detached ligands on the surface of NWs yield to the formation of bundles composed of individual NWs.

C. Complete degradation

This section is devoted to understanding how the green-light–emitting $CsPbBr_3$ bundles interact with water and become completely degraded. As shown in Fig. 5(a), further water treatment of the green-emitting phase having an intense PL signal at 500 nm results in transformation into another phase that has no optical activity. The optical image presented in Fig. 5(b) reveals that formation of these nonemitting crystal structures is accompanied by formation of white domains.

For understanding of the final structure in terms of a crystallographic perspective, XRD measurements were employed for white crystals, namely, nonemitting large bundles. XRD patterns of degraded and as-synthesized NWs, CsBr, and $PbBr_2$ are presented in Fig. 5(c). Identical reflections (15° and 30°) of perovskite, which indicate (110) and (004) planes, is still observed. The reflections of a degraded form may be assigned to residual NWs. However, according to additional reflections of degraded crystals, it can be said that the crystallographic nature shows alteration as much as transformation shows in morphology. Nevertheless, the additional reflections cannot be unambiguously attributed to raw materials (CsBr and $PbBr_2$), although several reflections (e.g., 38°, 48°, and 52°) are already matched.

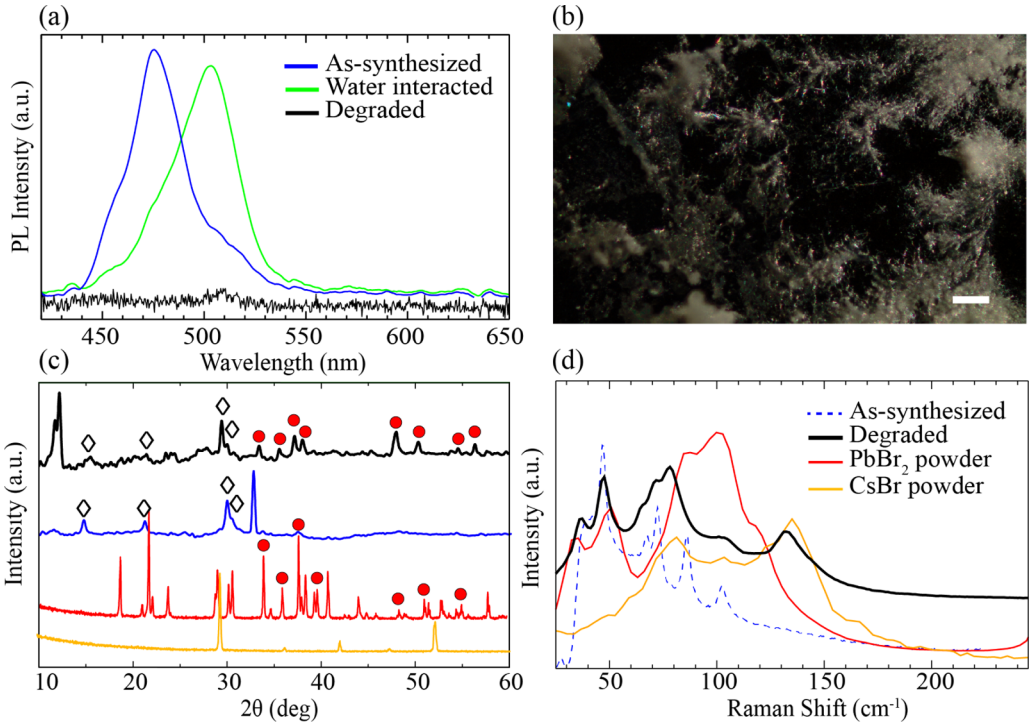

FIG. 5. (a) PL measurement of $CsPbBr_3$ NWs to degraded crystals, (b) optical image from nonemitting bundles, and (c) XRD pattern and (d) Raman measurement of $CsPbBr_3$ NWs, degraded crystals, CsPb, and $PbBr_2$ powder. Scale bar is 50 μm.

For further analysis of nonemitting regions, we also present the Raman spectrum of degraded regions of the crystal structure in Fig. 5(d). It is seen that the prominent Raman mode of $CsPbBr_3$ at 72 cm^{-1} is significantly decreased and has almost disappeared. Moreover, some novel modes, apparently stemming from the precursors $PbBr_2$ and CsBr, emerge at 38 and 130 cm^{-1} [64,65]. Therefore, as confirmed by the vibrational spectrum, complete degradation of $CsPbBr_3$ from the green-emitting phase occurs by turning the material into its constituents.

IV. CONCLUSIONS

In conclusion, we investigated how $CsPbBr_3$ perovskite is degraded by water using Raman, XRD, and PL measurements and state-of-the-art computational techniques. It is seen that during degradation even though no significant structural changes were visible with the naked eye, UV illumination reveals that the complete degradation takes place in two different steps: (1) transformation from NWs to bundles and (2) complete degradation from bundles to constituents. As verified by the first-principles calculations, competing interactions between water molecule oleic acid and oleilamine on the surface determine whether the structure crystallizes into a NW, bundle, or degraded form. Our PL, Raman, and XRD measurements also revealed that during the transition from the blue- to green-emitting phase of the $CsPbBr_3$ crystal symmetry remains the same. In the final step, complete degradation of $CsPbBr_3$ structure takes place by formation of CsPb and $PbBr_2$ powders. We believe that these results provide important advances in understanding the water-driven degradation of perovskite crystals and may construct a theoretical basis for fundamental investigations of their stability.

ACKNOWLEDGMENTS

Computational resources were provided by the TUBITAK ULAKBIM, High Performance and Grid Computing Center (TR-Grid e-Infrastructure). H.S. acknowledges financial support from the TUBITAK under Project No. 117F095.

[1] C. K. Møller, Nature (London) **182**, 1436 (1958).
[2] A. Kojima, K. Teshima, Y. Shirai, and T. Miyasaka, J. Am. Chem. Soc. **131**, 6050 (2009).
[3] C. C. Stoumpos and M. G. Kanatzidis, Acc. Chem. Res. **48**, 2791 (2015).
[4] D. Liu and T. L. Kelly, Nat. Photonics **8**, 133 (2014).
[5] H. Zhou, Q. Chen, G. Li, S. Luo, T.-b. Song, H.-S. Duan, Z. Hong, J. You, Y. Liu, and Y. Yang, Science **345**, 542 (2014).
[6] N. J. Jeon, J. H. Noh, W. S. Yang, Y. C. Kim, S. Ryu, J. Seo, and S. I. Seok, Nature (London) **517**, 476 (2015).
[7] J.-H. Im, C.-R. Lee, J.-W. Lee, S.-W. Park, and N.-G. Park, Nanoscale **3**, 4088 (2011).
[8] H. Cho, S.-H. Jeong, M.-H. Park, Y.-H. Kim, C. Wolf, C.-L. Lee, J. H. Heo, A. Sadhanala, N. Myoung, S. Yoo, S. H. Im, R. H. Friend, and T.-W. Lee, Science **350**, 1222 (2015).
[9] J. Byun, H. Cho, C. Wolf, M. Jang, A. Sadhanala, R. H. Friend, H. Yang, and T.-W. Lee, Adv. Mater. **28**, 7515 (2016).

[10] J. Li, L. Xu, T. Wang, J. Song, J. Chen, J. Xue, Y. Dong, B. Cai, Q. Shan, B. Han, and H. Zeng, Adv. Mater. **29**, 1603885 (2017).

[11] H. Zhu, Y. Fu, F. Meng, X. Wu, Z. Gong, Q. Ding, M. V. Gustafsson, M. T. Trinh, S. Jin, and X. Zhu, Nat. Mater. **14**, 636 (2015).

[12] S. Yakunin, L. Protesescu, F. Krieg, M. I. Bodnarchuk, G. Nedelcu, M. Humer, G. De Luca, M. Fiebig, W. Heiss, and M. V. Kovalenko, Nat. Commun. **6**, 8056 (2015).

[13] P. Ramasamy, D.-H. Lim, B. Kim, S.-H. Lee, M.-S. Lee, and J.-S. Lee, Chem. Commun. **52**, 2067 (2016).

[14] X. Li, F. Cao, D. Yu, J. Chen, Z. Sun, Y. Shen, Y. Zhu, L. Wang, Y. Wei, Y. Wu, and H. Zeng, Small **13**, 1603996 (2017).

[15] S. Bai, Z. Yuan, and F. Gao, J. Mater. Chem. C **4**, 3898 (2016).

[16] C. C. Stoumpos and M. G. Kanatzidis, Adv. Mater. **28**, 5778 (2016).

[17] X. Li, Y. Wu, S. Zhang, B. Cai, Y. Gu, J. Song, and H. Zeng, Adv. Funct. Mater. **26**, 2435 (2016).

[18] L. Protesescu, S. Yakunin, M. I. Bodnarchuk, F. Krieg, R. Caputo, C. H. Hendon, R. X. Yang, A. Walsh, and M. V. Kovalenko, Nano Lett. **15**, 3692 (2015).

[19] M. V. Kovalenko, L. Protesescu, and M. I. Bodnarchuk, Science **358**, 745 (2017).

[20] H. Huang, M. I. Bodnarchuk, S. V. Kershaw, M. V. Kovalenko, and A. L. Rogach, ACS Energy Lett. **2**, 2071 (2017).

[21] Y. Iso and T. Isobe, ECS J. Solid State Sci. Technol. **7**, R3040 (2018).

[22] H.-C. Wang, S.-Y. Lin, A.-C. Tang, B. P. Singh, H.-C. Tong, C.-Y. Chen, Y.-C. Lee, T.-L. Tsai, and R.-S. Liu, Angew. Chem. Int. Ed. **55**, 7924 (2016).

[23] S. Bhaumik, S. A. Veldhuis, Y. F. Ng, M. Li, S. K. Muduli, T. C. Sum, B. Damodaran, S. Mhaisalkar, and N. Mathews, Chem. Commun. **52**, 7118 (2016).

[24] Z.-J. Li, E. Hofman, J. Li, A. H. Davis, C.-H. Tung, L.-Z. Wu, and W. Zheng, Adv. Funct. Mater. **28**, 1704288 (2018).

[25] B. Qiao, P. Song, J. Cao, S. Zhao, Z. Shen, D. Gao, Z. Liang, Z. Xu, D. Song, and X. Xu, Nanotechnology **28**, 445602 (2017).

[26] H. Huang, B. Chen, Z. Wang, T. F. Hung, A. S. Susha, H. Zhong, and A. L. Rogach, Chem. Sci. **7**, 5699 (2016).

[27] B. Luo, Y.-C. Pu, S. A. Lindley, Y. Yang, L. Lu, Y. Li, X. Li, and J. Z. Zhang, Angew. Chem. **128**, 9010 (2016).

[28] Y. Wang, J. He, H. Chen, J. Chen, R. Zhu, P. Ma, A. Towers, Y. Lin, A. J. Gesquiere, S.-T. Wu, and Y. Dong, Adv. Mater. **28**, 10710 (2016).

[29] S. N. Raja, Y. Bekenstein, M. A. Koc, S. Fischer, D. Zhang, L. Lin, R. O. Ritchie, P. Yang, and A. P. Alivisatos, ACS Appl. Mater. Interfaces **8**, 35523 (2016).

[30] Y. Wei, X. Deng, Z. Xie, X. Cai, S. Liang, P. Ma, Z. Hou, Z. Cheng, and J. Lin, Adv. Funct. Mater. **27**, 1703535 (2017).

[31] S. Sun, D. Yuan, Y. Xu, A. Wang, and Z. Deng, ACS Nano **10**, 3648 (2016).

[32] X. Zhang, H. Lin, H. Huang, C. Reckmeier, Y. Zhang, W. C. Choy, and A. L. Rogach, Nano Lett. **16**, 1415 (2016).

[33] A. Swarnkar, R. Chulliyil, V. K. Ravi, M. Irfanullah, A. Chowdhury, and A. Nag, Angew. Chem. **127**, 15644 (2015).

[34] J. Xue, Y. Gu, Q. Shan, Y. Zou, J. Song, L. Xu, Y. Dong, J. Li, and H. Zeng, Angew. Chem. Int. Ed. **56**, 5232 (2017).

[35] M. Chen, Y. Zou, L. Wu, Q. Pan, D. Yang, H. Hu, Y. Tan, Q. Zhong, Y. Xu, H. Liu, B. Sun, and Q. Zhang, Adv. Funct. Mater. **27**, 1701121 (2017).

[36] G. Yuan, C. Ritchie, M. Ritter, S. Murphy, D. E. Gomez, and P. Mulvaney, J. Phys. Chem. C (2018), doi:10.1021/acs.jpcc.7b11168.

[37] T. Leijtens, K. Bush, R. Cheacharoen, R. Beal, A. Bowring, and M. D. McGehee, J. Mater. Chem. A **2**, 11483 (2017).

[38] J. Haruyama, K. Sodeyama, L. Han, and Y. Tateyama, J. Am. Chem. Soc. **137**, 10048 (2015).

[39] H. Kawai, G. Giorgi, A. Marini, and K. Yamashita, Nano Lett. **15**, 3103 (2015).

[40] W. Geng, L. Zhang, Y.-N. Zhang, W.-M. Lau, and L.-M. Liu, J. Phys. Chem. C **118**, 19565 (2014).

[41] W.-J. Yin, J.-H. Yang, J. Kang, Y. Yan, and S.-H. Wei, J. Mater. Chem. A **3**, 8926 (2015).

[42] F. Iyikanat, E. Sari, and H. Sahin, Phys. Rev. B **96**, 155442 (2017).

[43] J. Kang and L.-W. Wang, J. Phys. Chem. Lett. **8**, 489 (2017).

[44] W.-J. Yin, T. Shi, and Y. Yan, Appl. Phys. Lett. **104**, 063903 (2014).

[45] J. Kim, S.-H. Lee, J. H. Lee, and K.-H. Hong, J. Phys. Chem. Lett. **5**, 1312 (2014).

[46] J. M. Azpiroz, E. Mosconi, J. Bisquert, and F. De Angelis, Energy Environ. Sci. **8**, 2118 (2015).

[47] J. Haruyama, K. Sodeyama, I. Hamada, L. Han, and Y. Tateyama, J. Phys. Chem. Lett. **8**, 5840 (2017).

[48] Y. Bekenstein, B. A. Koscher, S. W. Eaton, P. Yang, and A. P. Alivisatos, J. Am. Chem. Soc. **137**, 16008 (2015).

[49] D. Amgar, A. Stern, D. Rotem, D. Porath, and L. Etgar, Nano Lett. **17**, 1007 (2017).

[50] G. Kresse and D. Joubert, Phys. Rev. B **59**, 1758 (1999).

[51] P. E. Blöchl, Phys. Rev. B **50**, 17953 (1994).

[52] G. Kresse and J. Hafner, Phys. Rev. B **47**, 558 (1993).

[53] G. Kresse and J. Furthmüller, Phys. Rev. B **54**, 11169 (1996).

[54] J. P. Perdew and A. Zunger, Phys. Rev. B **23**, 5048 (1981).

[55] D. M. Ceperley and B. J. Alder, Phys. Rev. Lett. **45**, 566 (1980).

[56] G. Henkelman, A. Arnaldsson, and H. Jónsson, Comput. Mater. Sci. **36**, 354 (2006).

[57] E. H. Smith, N. A. Benedek, and C. J. Fennie, Inorg. Chem. **54**, 8536 (2015).

[58] Y. Wang, X. Lu, W. Yang, T. Wen, L. Yang, X. Ren, L. Wang, Z. Lin, and Y. Zhao, J. Am. Chem. Soc. **137**, 11144 (2015).

[59] P. Cottingham and R. L. Brutchey, Chem. Commun. **52**, 5246 (2016).

[60] D. Zhang, S. W. Eaton, Y. Yu, L. Dou, and P. Yang, J. Am. Chem. Soc. **137**, 9230 (2015).

[61] D. M. Calistru, L. Mihut, S. Lefrant, and I. Baltog, J. Appl. Phys. **82**, 5391 (1997).

[62] Y. Zhang, M. I. Saidaminov, I. Dursun, H. Yang, B. Murali, E. Alarousu, E. Yengel, B. A. Alshankiti, O. M. Bakr, and O. F. Mohammed, J. Phys. Chem. Lett. **8**, 961 (2017).

[63] U. Thumu, L. Houben, H. Cohen, M. Menahem, I. Pinkas, L. Avram, T. Wolf, A. Teitelboim, M. Leskes, O. Yaffe, D. Oron, and M. Kazes, Chem. Mater. **30**, 84 (2017).

[64] L. Isupova and E. Sobolev, J. Struct. Chem. **9**, 263 (1968).

[65] B. Willemsen, J. Inorg. Nucl. Chem. **33**, 3963 (1971).